Physica B 592 (2020) 412260

Contents lists available at ScienceDirect

Physica B: Physics of Condensed Matter

journal homepage: www.elsevier.com/locate/physb

Geometric contribution to the Goldstone mode in spin–orbit coupled Fermi superfluids

M. Iskin

Department of Physics, Koç University, Rumelifeneri Yolu, 34450 Sarıyer, Istanbul, Turkey

ARTICLE INFO

Keywords:
BCS–BEC crossover
Spin–orbit coupling
Quantum metric tensor

ABSTRACT

The so-called quantum metric tensor is a band-structure invariant whose measure corresponds to the quantum distance between nearby states in the Hilbert space, characterizing the geometry of the underlying quantum states. In the context of spin–orbit coupled Fermi gases, we recently proposed that the quantum metric has a partial control over all those superfluid properties that depend explicitly on the mass of the superfluid carriers, i.e., the effective-mass tensor of the corresponding (two- or many-body) bound state. Here we scrutinize this finding by analyzing the collective phase and amplitude excitations at zero temperature. In particular to the Goldstone mode, we present extensive numerical calculations for the Weyl and Rashba spin–orbit couplings, revealing that, despite being small, the geometric contribution is solely responsible for the nonmonotonic evolution of the sound velocity in the BCS–BEC crossover.

1. Introduction

The quantum geometric tensor [1–3] lies at the heart of modern solid-state and condensed-matter physics: while it describes the local geometry of the underlying Bloch states, it can be related to the global properties of some systems in most peculiar ways. For instance, its imaginary part corresponds to the Berry curvature measuring the emergent gauge field in momentum space, and it can be associated with the topological invariants that are used to classify quantum Hall states or topological insulators [4,5]. In contrast, its real part corresponds to the quantum metric tensor measuring the quantum distance/fidelity between nearby Bloch states, and it can be associated with, e.g., the density and the effective-mass tensor of the superfluid (SF) carriers in spin–orbit coupled Fermi gases [6,7], as well as with many other systems [8–10].

In the context of multi-band superconductivity, the new surge of theoretical interest in quantum-metric effects dates back only to 2015, soon after its direct association with the geometric origin of superfluidity in topologically nontrivial flat bands [11]. It was found that the SF weight (also known as the SF stiffness tensor) has two distinct contributions based on the physical mechanisms involved. In addition to the conventional contribution that is controlled by the electronic spectra of the Bloch bands, there is also the so-called geometric contribution coming from the interband processes [11,12]. It later turns out that the quantum geometry has a partial control not only over the SF weight but also over all those SF properties that depend explicitly on the effective-mass tensor of the corresponding (two- or many-body) bound state [7]. There have been many studies on the subject exploring a variety of multi-band Hamiltonians, including most recently that of the twisted bilayer graphene [13–15].

Motivated by the ongoing experimental progress [16–20] and given our recent findings [6,7,21], here we consider a two-component Fermi gas with an arbitrary spin–orbit coupling (SOC), and analyze its collective excitations in the BCS–BEC crossover. We show that the velocity of the Goldstone mode has two contributions as well: in addition to the conventional intraband one that is controlled by the helicity spectrum, the geometric interband contribution is controlled by the quantum metric. We present extensive numerical calculations for the Weyl and Rashba SOCs revealing that, despite being much smaller than the conventional one, the geometric contribution is solely responsible for the nonmonotonic evolution of the sound velocity in the BCS–BEC crossover.

The rest of this paper is organized as follows. In Section 2, after introducing the many-body Hamiltonian, we first describe the effective-Gaussian action for the phase- and amplitude-only degrees of freedoms, and then derive analytical expressions for the collective modes with a special emphasis on the distinction between the conventional and geometric contributions. Much of the theoretical details on the effective-action approach are deferred to Appendix. The resultant Goldstone (phase) mode is analyzed Section 3, where we present numerical results for a 3D Fermi gas with a Weyl or a Rashba SOC, and for a 2D Fermi gas with a Rashba SOC for completeness. We end the paper with a brief summary of our conclusions in Section 4.

E-mail address: miskin@ku.edu.tr.

https://doi.org/10.1016/j.physb.2020.412260
Received 19 February 2020; Received in revised form 31 March 2020; Accepted 8 May 2020
Available online 12 May 2020

2. Collective excitations

Having a two-component (↑ and ↓) Fermi gas with an arbitrary SOC that is driven across an s-wave Feshbach resonance in mind, we consider the Hamiltonian

$$H = \sum_{\mathbf{k}} (a^\dagger_{\uparrow\mathbf{k}}\, a^\dagger_{\downarrow\mathbf{k}}) \left[\xi_{\mathbf{k}}\sigma_0 + \mathbf{d}_{\mathbf{k}}\cdot\boldsymbol{\sigma}\right] \begin{pmatrix} a_{\uparrow\mathbf{k}} \\ a_{\downarrow\mathbf{k}} \end{pmatrix} - U \sum_{\mathbf{k}\mathbf{k}'\mathbf{q}} a^\dagger_{\uparrow,\mathbf{k}+\mathbf{q}/2} a^\dagger_{\downarrow,-\mathbf{k}+\mathbf{q}/2} a_{\downarrow,-\mathbf{k}'+\mathbf{q}/2} a_{\uparrow,\mathbf{k}'+\mathbf{q}/2}, \tag{1}$$

where $a^\dagger_{\sigma\mathbf{k}}$ ($a_{\sigma\mathbf{k}}$) creates (annihilates) a pseudospin-σ fermion with momentum $\mathbf{k}$, i.e., in units of $\hbar \to 1$ the Planck constant. In the first line, $\xi_{\mathbf{k}} = \epsilon_{\mathbf{k}} - \mu$ is the usual free-particle dispersion $\epsilon_{\mathbf{k}} = k^2/(2m)$ shifted by the chemical potential μ, $\mathbf{d}_{\mathbf{k}} = \sum_i d^i_{\mathbf{k}}\hat{\boldsymbol{\imath}}$ is the SOC field with $\hat{\boldsymbol{\imath}}$ denoting the unit vector along the $i = (x, y, z)$ direction, σ_0 is a 2×2 identity matrix, and $\boldsymbol{\sigma} = \sum_i \sigma_i\hat{\boldsymbol{\imath}}$ is a vector of Pauli spin matrices. Our notation is such that $d^i_{\mathbf{k}} = \alpha_i k_i$ corresponds to the Weyl SOC when $\alpha_i = \alpha$ for all i, and to the Rashba SOC when $\alpha_z = 0$. We choose $\alpha \geq 0$ without the loss of generality. Thus, the one-body problem is described by the Hamiltonian density $h^0_{\mathbf{k}} = \epsilon_{\mathbf{k}}\sigma_0 + \mathbf{d}_{\mathbf{k}}\cdot\boldsymbol{\sigma}$, determining the helicity spectrum $\epsilon_{s\mathbf{k}} = \epsilon_{\mathbf{k}} + s d_{\mathbf{k}}$ and the helicity eigenstates $|s\mathbf{k}\rangle$ via the wave equation $h^0_{\mathbf{k}}|s\mathbf{k}\rangle = \epsilon_{s\mathbf{k}}|s\mathbf{k}\rangle$. Here, $s = \pm$ labels the helicity bands, $d_{\mathbf{k}} = |\mathbf{d}_{\mathbf{k}}|$, and the unit vector $\hat{\mathbf{d}}_{\mathbf{k}} = \mathbf{d}_{\mathbf{k}}/d_{\mathbf{k}}$ plays an important role throughout the paper.

In the second line of Eq. (1), $U \geq 0$ corresponds to the strength of the zero-ranged density–density interactions between ↑ and ↓ particles, and we tackle this term by making use of the imaginary-time functional path-integral formalism for the paired fermions. This formalism offers a systematic approach to go beyond the mean-field theory as the fluctuation effects can be incorporated into the effective action order by order as a power-series expansion around the stationary saddle-point [22–27]. As shown in the Appendix, the zeroth-order (i.e., the saddle-point) action coincides with the mean-field one, and can be written as

$$S_0 = \frac{\Delta_0^2}{TU} + \sum_{s\mathbf{k}} \left\{ \frac{\xi_{s\mathbf{k}} - E_{s\mathbf{k}}}{2T} + \ln[f(-E_{s\mathbf{k}})] \right\}, \tag{2}$$

where $\Delta_0 = U\langle a_{\uparrow\mathbf{k}} a_{\downarrow,-\mathbf{k}}\rangle$ is the saddle-point order parameter with $\langle\dots\rangle$ denoting a thermal average, T is the temperature in units of $k_B \to 1$ the Boltzmann constant, $E_{s\mathbf{k}} = \sqrt{\xi^2_{s\mathbf{k}} + \Delta_0^2}$ is the quasiparticle energy spectrum associated with $\xi_{s\mathbf{k}} = \epsilon_{s\mathbf{k}} - \mu$, and $f(x) = 1/(e^{x/T} + 1)$ is the Fermi–Dirac distribution. Here, we take Δ_0 to be a real parameter without the loss of generality, and determine its value by imposing the saddle-point condition $\partial S_0/\partial\Delta_0 = 0$ on the order parameter, leading to

$$1 = U \sum_{s\mathbf{k}} \frac{1 - 2f(E_{s\mathbf{k}})}{4E_{s\mathbf{k}}}. \tag{3}$$

Furthermore, μ is determined by the thermodynamic relation $N_0 = -T\partial S_0/\partial\mu$ for the number of particles, leading to

$$N_0 = \sum_{s\mathbf{k}} \left\{ \frac{1}{2} - \frac{\xi_{s\mathbf{k}}}{2E_{s\mathbf{k}}}[1 - 2f(E_{s\mathbf{k}})] \right\}. \tag{4}$$

These saddle-point equations constitute the self-consistent BCS–BEC crossover theory for pairing, and they coincide with those of the mean-field approximation. The coupled solutions for Δ_0 and μ have served as a reliable guide for the cold-atom community, providing a qualitative description of the SF state at sufficiently low temperatures across an s-wave Feshbach resonance [22–27].

Going beyond S_0 in the Appendix, we first introduce the bosonic field $\Delta_q = \Delta_0 + \Lambda_q$, where Λ_q corresponds to the fluctuations of the order parameter around its stationary value Δ_0 with the collective index $q = (\mathbf{q}, i\nu_n)$ denoting both the pair momentum $\mathbf{q}$ and the bosonic Matsubara frequency $\nu_n = 2\pi nT$, and then derive the effective-Gaussian action $S_{\rm Gauss} = S_0 + S_2$. Note that the first order term S_1 vanishes thanks to the saddle-point condition on the order parameter. Furthermore, it is physically insightful to separate the phase and amplitude degrees of freedoms through the unitary transformation $\Lambda_q = (\lambda_q + i\theta_q)/\sqrt{2}$, leading to a phase-only action S^θ_2 and to a amplitude-only one S^λ_2 that are of the form

$$S^\theta_2 = \frac{1}{2T}\sum_q \theta^*_q \left[M^{11}_{q,E} - M^{12}_q - \frac{(M^{11}_{q,O})^2}{M^{11}_{q,E} + M^{12}_q} \right] \theta_q, \tag{5}$$

$$S^\lambda_2 = \frac{1}{2T}\sum_q \lambda^*_q \left[M^{11}_{q,E} + M^{12}_q - \frac{(M^{11}_{q,O})^2}{M^{11}_{q,E} - M^{12}_q} \right] \lambda_q. \tag{6}$$

Here, since $M^{11}_{q,O}$ couples the phase and amplitude modes, the phase-only action is derived by integrating out the amplitude fields, and vice versa [23]. It turns out that the phase and amplitude modes are generally coupled to each other except for the strict BCS limit where $B^2 \ll AR$ (see the dispersions below). Therefore, we would like to remark here that the resulting response of our phase-only action is not due to the purely phase fluctuations, and vice versa. While the thermal expressions for the matrix elements M^{ij}_q of the inverse-fluctuation propagator $\mathbf{M}_q$ are given in the Appendix, here we restrict ourselves to the collective excitations on top of the thermal ground state. Thus, setting $T = 0$, and denoting $\xi_{s,\mathbf{k}+\mathbf{q}/2}$ by ξ; $\xi_{s',-\mathbf{k}+\mathbf{q}/2}$ by ξ'; $E_{s,\mathbf{k}+\mathbf{q}/2}$ by E; $E_{s',-\mathbf{k}+\mathbf{q}/2}$ by E'; and $\hat{\mathbf{d}}_{\pm\mathbf{k}+\mathbf{q}/2}$ by $\hat{\mathbf{d}}_\pm$, a compact way to write the matrix elements is [23]

$$M^{11}_{q,E} = \frac{1}{U} + \sum_{ss'\mathbf{k}} \frac{(\xi\xi' + EE')(E + E')(1 - ss'\hat{\mathbf{d}}_+\cdot\hat{\mathbf{d}}_-)}{8EE'[(i\nu_n)^2 - (E + E')^2]}, \tag{7}$$

$$M^{11}_{q,O} = \sum_{ss'\mathbf{k}} \frac{(\xi E' + E\xi')i\nu_n(1 - ss'\hat{\mathbf{d}}_+\cdot\hat{\mathbf{d}}_-)}{8EE'[(i\nu_n)^2 - (E + E')^2]}, \tag{8}$$

$$M^{12}_q = -\sum_{ss'\mathbf{k}} \frac{\Delta_0^2(E + E')(1 - ss'\hat{\mathbf{d}}_+\cdot\hat{\mathbf{d}}_-)}{8EE'[(i\nu_n)^2 - (E + E')^2]}. \tag{9}$$

Here, $M^{11}_{q,E}$ and M^{12}_q are even functions of $i\nu_n$, but $M^{11}_{q,O}$ is an odd one.

The dispersions $\omega_{\mathbf{q}}$ for the collective modes are determined by the poles of the propagator matrix $\mathbf{M}^{-1}_q$ for the pair fluctuation fields, i.e., $\omega^\theta_{\mathbf{q}}$ for the phase mode and $\omega^\lambda_{\mathbf{q}}$ for the amplitude one are determined, respectively, by setting $[\dots] = 0$ in Eqs. (5) and (6) after an analytic continuation $i\nu_n \to \omega + i0^+$ to the real axis [22–27]. For this purpose, it is sufficient to retain terms that are up to quadratic orders in their small $\mathbf{q}$ and ω expansions [28], i.e.,

$$M^{11}_{q,E} + M^{12}_q = A + \sum_{ij} C_{ij} q_i q_j - D\omega^2 + \cdots, \tag{10}$$

$$M^{11}_{q,E} - M^{12}_q = \sum_{ij} Q_{ij} q_i q_j - R\omega^2 + \cdots, \tag{11}$$

$$M^{11}_{q,O} = -B\omega + \cdots. \tag{12}$$

This calculation leads to a gapless phase (Goldstone) mode $(\omega^\theta_{\mathbf{q}})^2 = \sum_{ij} x_{ij} q_i q_j$ with

$$x_{ij} = \frac{Q_{ij}}{R + B^2/A} \tag{13}$$

for the phase-only action, and to a gapped amplitude (Higgs) mode $(\omega^\lambda_{\mathbf{q}})^2 = \omega_0^2 + \sum_{ij} y_{ij} q_i q_j$ with

$$\omega_0 = \sqrt{\frac{A + B^2/R}{D}}, \tag{14}$$

$$y_{ij} = \frac{C_{ij}}{D} + \frac{Q_{ij}}{R + R^2A/B^2} \tag{15}$$

for the amplitude-only action. Notice that the velocities of the modes have a tensor structure in general, and can be anisotropic depending on the $\mathbf{k}$-space structure of the SOC. We are interested only in the low-energy Goldstone mode at $T = 0$ since this mode is not damped for all $U \neq 0$ provided that the quasiparticle excitations $E_{s\mathbf{k}}$ are gapped for all $\Delta_0 \neq 0$ [29].

It turns out that the general expressions for the nonkinetic-expansion coefficients can simply be written as a sum over their well-known counterparts for the usual one-band problem, i.e.,

$$A = \sum_{s\mathbf{k}} \frac{\Delta_0^2}{4E_{s\mathbf{k}}^3}, \tag{16}$$

$$B = \sum_{s\mathbf{k}} \frac{\xi_{s\mathbf{k}}}{8E_{s\mathbf{k}}^3}, \tag{17}$$

$$D = \sum_{s\mathbf{k}} \frac{\xi_{s\mathbf{k}}^2}{16E_{s\mathbf{k}}^5}, \tag{18}$$

$$R = \sum_{s\mathbf{k}} \frac{1}{16E_{s\mathbf{k}}^3} \tag{19}$$

are due entirely to intraband mechanisms [22–27]. Motivated by the recent findings [6,7,21], and to gain more physical insight, we divide the kinetic-expansion coefficients into two distinct contributions $Q_{ij} = Q_{ij}^{\text{intra}} + Q_{ij}^{\text{inter}}$ and $C_{ij} = C_{ij}^{\text{intra}} + C_{ij}^{\text{inter}}$, based on their physical origins, i.e., depending on whether intraband or interband processes are involved. For instance, a compact way to write their intraband (i.e., conventional) contributions is

$$Q_{ij}^{\text{intra}} = \sum_{s\mathbf{k}} \frac{1}{16E_{s\mathbf{k}}^3} \frac{\partial \xi_{s\mathbf{k}}}{\partial k_i} \frac{\partial \xi_{s\mathbf{k}}}{\partial k_j}, \tag{20}$$

$$C_{ij}^{\text{intra}} = \sum_{s\mathbf{k}} \frac{1}{16E_{s\mathbf{k}}^3} \left(1 - \frac{5\Delta_0^2 \xi_{s\mathbf{k}}^2}{E_{s\mathbf{k}}^4}\right) \frac{\partial \xi_{s\mathbf{k}}}{\partial k_i} \frac{\partial \xi_{s\mathbf{k}}}{\partial k_j}. \tag{21}$$

We note that these terms can be transformed into their more familiar but more involved forms [22,30] through first writing $\partial[(\partial\xi_{s\mathbf{k}}/\partial k_j)/E_{s\mathbf{k}}^3]/\partial k_i = [\partial^2\xi_{s\mathbf{k}}/(\partial k_i \partial k_j)]/E_{s\mathbf{k}}^3 - 3(\partial\xi_{s\mathbf{k}}/\partial k_i)(\partial\xi_{s\mathbf{k}}/\partial k_j)\xi_{s\mathbf{k}}/E_{s\mathbf{k}}^5$, and then identifying $\sum_{\mathbf{k}} \xi_{s\mathbf{k}} \partial[(\partial\xi_{s\mathbf{k}}/\partial k_j)/E_{s\mathbf{k}}^3]/\partial k_i \equiv -\sum_{\mathbf{k}} (\partial\xi_{s\mathbf{k}}/\partial k_i)(\partial\xi_{s\mathbf{k}}/\partial k_j)/E_{s\mathbf{k}}^3$ after an integration by parts, and hence the name conventional. On the other hand, a compact way to write their interband (i.e., geometric) contributions is

$$Q_{ij}^{\text{inter}} = -\sum_{s\mathbf{k}} \frac{d_{\mathbf{k}}}{8s\xi_{\mathbf{k}} E_{s\mathbf{k}}} g_{\mathbf{k}}^{ij}, \tag{22}$$

$$C_{ij}^{\text{inter}} = -\sum_{s\mathbf{k}} \frac{d_{\mathbf{k}}}{8s\xi_{\mathbf{k}} E_{s\mathbf{k}}} \left(1 + \frac{2\Delta_0^2}{d_{\mathbf{k}}^2}\right) g_{\mathbf{k}}^{ij}, \tag{23}$$

where $g_{\mathbf{k}}^{ij} = (1/2)\lim_{\mathbf{q}\to\mathbf{0}} \partial^2(\hat{\mathbf{d}}_+ \cdot \hat{\mathbf{d}}_-)/(\partial q_i \partial q_j)$ or equivalently $g_{\mathbf{k}}^{ij} = (\partial\hat{\mathbf{d}}_{\mathbf{k}}/\partial k_i)\cdot(\partial\hat{\mathbf{d}}_{\mathbf{k}}/\partial k_j)/2$ is the total quantum metric tensor of the helicity bands [6,7]. Alternatively, the quantum metric can be written as $g_{\mathbf{k}}^{ij} = [\sum_{\ell}(\partial d_{\mathbf{k}}^{\ell}/\partial k_i)(\partial d_{\mathbf{k}}^{\ell}/\partial k_j) - (\partial d_{\mathbf{k}}/\partial k_i)(\partial d_{\mathbf{k}}/\partial k_j)]/(2d_{\mathbf{k}}^2)$, reducing to

$$g_{\mathbf{k}}^{ij} = \alpha_i \alpha_j \left(\frac{\delta_{ij}}{2d_{\mathbf{k}}^2} - \frac{d_{\mathbf{k}}^i d_{\mathbf{k}}^j}{2d_{\mathbf{k}}^4}\right) \tag{24}$$

for the specific case when $d_{\mathbf{k}}^i = \alpha_i k_i$. Since the interband contributions are directly controlled by the geometry of the underlying quantum states in the parameter ($\mathbf{k}$) space, we refer to them as the geometric ones.

All of the coefficients A, B, C_{ij}, etc., are derived at $T = 0$ for arbitrary U and $\mathbf{d}_{\mathbf{k}}$, and can be used both in two and three dimensions. Next we present their specific application to three systems that are of immediate experimental and/or theoretical interest: (i) a 3D Fermi gas with a Weyl SOC, (ii) a 3D Fermi gas with a Rashba SOC, and (iii) a 2D Fermi gas with a Rashba SOC.

3. Numerical results

In this paper, our primary interest is in the cooperation and/or competition between the conventional intraband contribution $x_{ij}^{\text{intra}} = Q_{ij}^{\text{intra}}/(R + B^2/A)$ and the geometric interband one $x_{ij}^{\text{inter}} = Q_{ij}^{\text{inter}}/(R + B^2/A)$ on the velocity of the Goldstone mode. For this purpose, one first needs to obtain a self-consistent solution for Δ_0 and μ by coupling the saddle-point condition and the saddle-point number equation, and then plug these solutions into the coefficients.

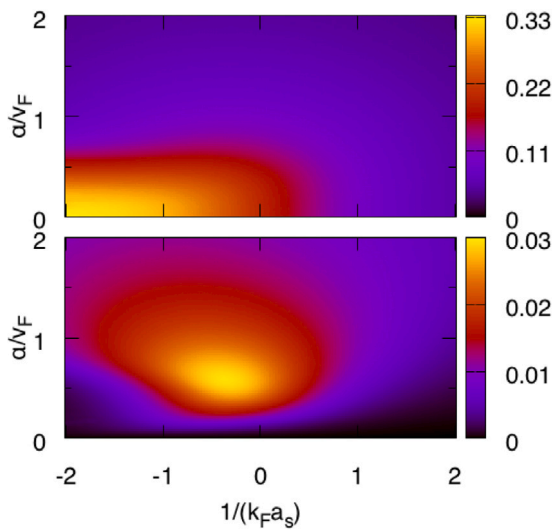

Fig. 1. A 3D Fermi gas with Weyl SOC is mapped at $T = 0$ in the plane of two-body scattering length a_s and SOC strength α. Square of the sound velocity x_0/v_F^2 is shown (upper panel) along with its geometric contribution x_0^{inter}/v_F^2 (lower panel).

For instance, in Fig. 1, we show $x_{ij} = x_0\delta_{ij}$ for a 3D Fermi gas with a Weyl SOC, where $\mathbf{d}_{\mathbf{k}} = \alpha\mathbf{k}$, and therefore, $x_0 = x_0^{\text{intra}} + x_0^{\text{inter}}$ is isotropic in the entire $\mathbf{q}$ space with δ_{ij} a Kronecker-delta. In accordance with the cold-atom literature, the two-body s-wave scattering length a_s in vacuum is substituted in this figure for U via the usual relation $V/U = -mV/(4\pi a_s) + \sum_{\mathbf{k}} 1/(2\epsilon_{\mathbf{k}})$, where V is the volume of the system. Furthermore, we choose $N = k_F^3 V/(3\pi^2)$ for the number of particles, and use the Fermi momentum k_F and the Fermi velocity $v_F = k_F/m$ as the relevant length and velocity scales in our numerical calculations. This is such that increasing U from 0 changes the dimensionless parameter $1/(k_F a_s)$ continuously from $-\infty$ to 0 to $+\infty$ in the BCS–BEC crossover.

In the weak-SOC limit when $\alpha/v_F \ll 1$, we recover the usual problem where x_0/v_F^2 is known to be a monotonically decreasing function of $1/(k_F a_s)$ with the well-known limits, i.e., 1/3 in the BCS regime and $k_F a_s/(3\pi)$ in the BEC regime [22,23]. Note that since the geometric contribution x_0^{inter} is originating from the interband processes, it plays a negligible role when $\alpha/v_F \to 0$. On the other hand, for intermediate α/v_F values, we find that x_0/v_F^2 is a nonmonotonic function of $1/(k_F a_s)$, exhibiting a noticeable peak in the crossover region around the unitarity [24–27]. This result is quite a surprise given that all of the ground-state properties are found to be monotonic functions of $1/(k_F a_s)$ for the usual BCS–BEC crossover problem with s-wave interactions [22]. In comparison to the dominant contribution from x_0^{intra}, our study reveals that, despite being small, the contribution from x_0^{inter} is sizeable enough to cause such a significant difference in x_0. Thus, even though a direct observation of x_0^{inter} may not be possible, realization of a nonmonotonic x_0 that is shown in Fig. 2 may be considered as the ultimate evidence for its subleading role.

Similarly, in Fig. 3, we show $x_{ij} = x_{ii}\delta_{ij}$ for a 3D Fermi gas with a Rashba SOC, where $\mathbf{d}_{\mathbf{k}} = \alpha\mathbf{k}_\perp$ with $\mathbf{k}_\perp = k_x\hat{\mathbf{x}} + k_y\hat{\mathbf{y}}$, and therefore, $x_\perp = x_\perp^{\text{intra}} + x_\perp^{\text{inter}}$ is still isotropic in $q_x q_y$ plane but it differs from that $x_{zz} = x_{zz}^{\text{intra}}$ of the q_z direction with $x_{zz}^{\text{inter}} = 0$. Note that since $g_{\mathbf{k}}^{iz} = 0$ for a Rashba SOC, all of the matrix elements x_{iz}^{inter} trivially vanish, leading to the aforementioned anisotropy. For intermediate α/v_F values, we again find that $x_\perp/v_F^2$ is a nonmonotonic function of $1/(k_F a_s)$, exhibiting a noticeable peak in the crossover region around the unitarity. However, x_{zz}/v_F^2 turns out to be a monotonic one no matter what α/v_F is. Thus, the dramatic difference between $x_\perp$ and x_{zz} may be used as an ultimate evidence for the presence of an interband contribution to the former, reflecting the geometry of the underlying quantum states.

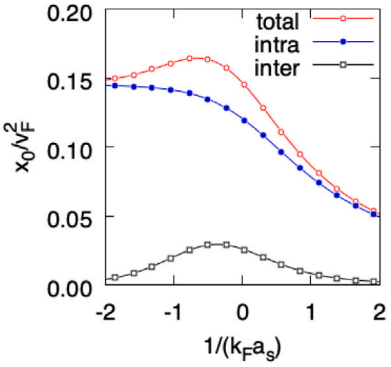

Fig. 2. Square of the sound velocity x_0/v_F^2 along with its intraband and geometric contributions are shown for a Weyl SOC when $\alpha = 0.6v_F$, i.e., this figure corresponds to a horizontal cut of Fig. 1 at $\alpha/v_F = 0.6$.

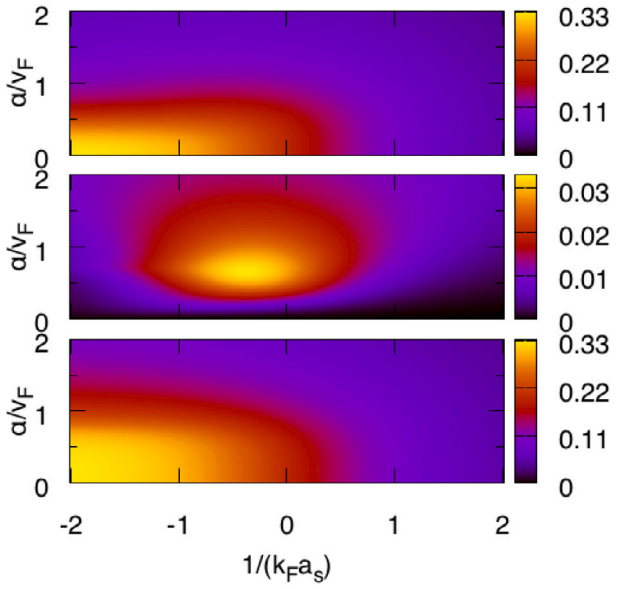

Fig. 3. A 3D Fermi gas with Rashba SOC is mapped at $T = 0$ in the plane of two-body scattering length a_s and SOC strength α. Square of the sound velocities $x_\perp/v_F^2$ and x_{zz}/v_F^2 are shown (upper and lower panels) along with the geometric contribution $x_\perp^{\text{inter}}/v_F^2$ (middle panel) of the former.

For completeness, in Fig. 4, we show $x_{ij} = x_0\delta_{ij}$ for a 2D Fermi gas with a Rashba SOC, where $\mathbf{d_k} = \alpha\mathbf{k}$, and therefore, $x_0 = x_0^{\text{intra}} + x_0^{\text{inter}}$ is isotropic in the entire $\mathbf{q}$ space. In accordance with the cold-atom literature, the two-body binding energy $\epsilon_b \geq 0$ in vacuum is substituted in this figure for U via the usual relation $A/U = \sum_{\mathbf{k}} 1/(2\epsilon_{\mathbf{k}} + \epsilon_b)$, where A is the area of the system. Furthermore, we choose $N = k_F^2 A/(2\pi)$, and use the Fermi energy $\epsilon_F = k_F^2/(2m)$ as the relevant energy scale in our numerical calculations. This is such that increasing U from 0 increases ϵ_b/ϵ_F continuously from 0 to ∞ in the BCS–BEC crossover. In the weak-SOC limit when $\alpha/v_F \ll 1$, we again recover the usual problem where x_0/v_F^2 is known to be 1/2 for all ϵ_b/ϵ_F, i.e., it remains a constant in the entire BCS–BEC crossover [23]. In contrast to the 3D results shown in Figs. 1 and 3 where the geometric contribution x_0^{inter} plays important roles only in the crossover region with a rapid decay in the BCS and BEC regimes, here x_0^{inter} retains its strength for most ϵ_b/ϵ_F values except for the extreme BCS limit when $\epsilon_b/\epsilon_F \ll 1$. Even then we find that the fraction x_0^{inter}/x_0 does not grow much, and saturates around a quarter.

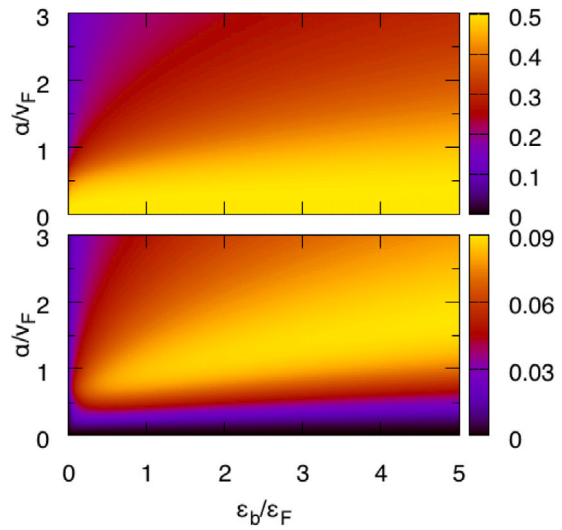

Fig. 4. A 2D Fermi gas with Rashba SOC is mapped at $T = 0$ in the plane of two-body binding energy ϵ_b and SOC strength α. Square of the sound velocity x_0/v_F^2 is shown (upper panel) along with its geometric contribution x_0^{inter}/v_F^2 (lower panel).

4. Conclusion

In summary, here we considered a two-component Fermi gas with an arbitrary SOC, and analyzed its collective excitations in the BCS–BEC crossover. Motivated by the recent findings [6,7], we divided the velocity of the Goldstone mode into two distinct contributions based on the physical mechanisms involved. While the conventional (intraband) contribution is controlled by the **k**-space derivatives of the helicity (one-body) spectrum, the geometric (interband) one is controlled by the **k**-space derivatives of the helicity eigenstates or the so-called quantum metric tensor characterizing the geometry of the underlying quantum states. We presented extensive numerical calculations for the Weyl and Rashba SOCs revealing that, despite being much smaller than the conventional one, the geometric contribution is solely responsible for the nonmonotonic evolution of the mode velocity in the BCS–BEC crossover.

These findings for the Goldstone mode in spin–orbit coupled Fermi gases are in complete agreement with our recent works that the quantum metric tensor has a subleading control over all those SF properties that depend explicitly on the effective-mass tensor of the corresponding (two- or many-body) bound state [6,7]. We note that whether the quantum-metric contribution can be isolated from the total is far from being clear with the current experimental techniques involving spin–orbit coupling. However, in the same spirit, given that the starting Hamiltonian Eq. (1) is quite generic, our analytical expressions for the Goldstone mode may also find direct applications in other contexts that exhibit a two-band band structure. In particular, it is desirable to study the Goldstone mode in a narrow- or a flat-band system [31,32], for which the geometric contribution is expected to take the lead. We note that since the lower helicity band is partially flat in momentum space, the geometric contribution turns out to be not very large in the case of spin–orbit coupled Fermi SFs. As a final remark, our work suggests that an analogous contribution to the collective excitations must be present in many other multi-band systems including the twisted bilayer graphene.

Declaration of competing interest

The authors declare that they have no known competing financial interests or personal relationships that could have appeared to influence the work reported in this paper.

Acknowledgment

This work is supported by the funding from TÜBİTAK Grant No. 1001-118F359.

Appendix. Effective-action approach

The imaginary-time functional path-integral formalism allows a systematic derivation of the effective action in the form of a power-series expansion of the fluctuations of the order parameter around its saddle-point value [22–27]. In this approach, to decouple the interaction term that is quartic in the fermionic degrees of freedom, one first uses a Hubbard–Stratonovich transformation at the expense of introducing a bosonic field Δ_q, and then integrates out the remaining terms that are quadratic in the fermionic degrees of freedom. Finally, by decomposing $\Delta_q = \Delta_0 + \Lambda_q$ in terms of a q-independent stationary field Δ_0 and q-dependent fluctuations around it, one may in principle obtain an effective action at the desired order in Λ_q. Here we include the first non-trivial term and obtain the effective-Gaussian action $S_{\rm Gauss} = S_0 + S_2$, as the first-order term S_1 trivially vanishes thanks to the saddle-point condition given in the main text.

For our interests, the zeroth-order action in Λ_q can be written as $S_0 = \Delta_0^2/(TU) + \sum_{s\mathbf{k}} \xi_{s\mathbf{k}}/(2T) - (1/2)\sum_k \ln[\det(\mathbf{G}_k^{-1}/T)]$, where the collective index $k = (\mathbf{k}, i\omega_\ell)$ denotes both the particle momentum $\mathbf{k}$ and the fermionic Matsubara frequency $\omega_\ell = (2\ell+1)\pi T$ [22–27]. Here, $\mathbf{G}_k^{-1} = i\omega_\ell \mathbf{1} - H_{\mathbf{k}}^0$ is the inverse Green's function for the saddle-point Hamiltonian $H_{\mathbf{k}}^0$, i.e.,

$$\mathbf{G}_k^{-1} = \begin{bmatrix} (i\omega_\ell - \xi_{\mathbf{k}})\sigma_0 - \mathbf{d}_{\mathbf{k}}\cdot\boldsymbol{\sigma} & i\Delta_0\sigma_y \\ -i\Delta_0\sigma_y & (i\omega_\ell + \xi_{\mathbf{k}})\sigma_0 - \mathbf{d}_{\mathbf{k}}\cdot\boldsymbol{\sigma}^* \end{bmatrix},$$

determining the quasiparticle and quasihole energies through $\det \mathbf{G}_k^{-1} = [(i\omega_\ell)^2 - E_{+,\mathbf{k}}^2][(i\omega_\ell)^2 - E_{-,\mathbf{k}}^2] = 0$, leading to $E_{s\mathbf{k}} = \sqrt{\xi_{s\mathbf{k}}^2 + \Delta_0^2}$ for the former. Performing the summation over the fermionic Matsubara frequency leads to the saddle-point action given in Eq. (2) of the main text.

The second-order term in Λ_q can be written as $S_2 = \sum_q |\Lambda_q|^2/(TU) + (1/4)\mathrm{Tr}\sum_{kq} \mathbf{G}_k \boldsymbol{\Sigma}_q \mathbf{G}_{k+q} \boldsymbol{\Sigma}_{-q}$, where Tr denotes a trace over the particle/hole and spin sectors, and the collective index $q = (\mathbf{q}, i\nu_n)$ denotes both the pair momentum $\mathbf{q}$ and the bosonic Matsubara frequency $\nu_n = 2\pi n T$ [23]. Here, the matrix elements of the Green's function $\mathbf{G}_k$ can be written as

$$G_k^{11} = \frac{1}{2}\sum_s \frac{i\omega_\ell + \xi_{s\mathbf{k}}}{(i\omega_\ell)^2 - E_{s\mathbf{k}}^2}\left(\sigma_0 + s\hat{\mathbf{d}}_{\mathbf{k}}\cdot\boldsymbol{\sigma}\right), \tag{A.1}$$

$$G_k^{22} = \frac{1}{2}\sum_s \frac{i\omega_\ell - \xi_{s\mathbf{k}}}{(i\omega_\ell)^2 - E_{s\mathbf{k}}^2}\left(\sigma_0 - s\hat{\mathbf{d}}_{\mathbf{k}}\cdot\boldsymbol{\sigma}^*\right), \tag{A.2}$$

$$G_k^{12} = \frac{1}{2}\sum_s \frac{-i\Delta_0\sigma_y}{(i\omega_\ell)^2 - E_{s\mathbf{k}}^2}\left(\sigma_0 - s\hat{\mathbf{d}}_{\mathbf{k}}\cdot\boldsymbol{\sigma}^*\right), \tag{A.3}$$

$$G_k^{21} = \frac{1}{2}\sum_s \frac{i\Delta_0\sigma_y}{(i\omega_\ell)^2 - E_{s\mathbf{k}}^2}\left(\sigma_0 + s\hat{\mathbf{d}}_{\mathbf{k}}\cdot\boldsymbol{\sigma}\right), \tag{A.4}$$

and those of the fluctuations $\boldsymbol{\Sigma}_q$ are $\Sigma_q^{11} = \Sigma_q^{22} = 0$, $\Sigma_q^{12} = i\Lambda_q\sigma_y$ and $\Sigma_q^{21} = -i\Lambda_{-q}^*\sigma_y$ [33,34]. After a lengthy but a straightforward summation over the fermionic Matsubara frequency, we find $S_2 = [1/(2T)]\sum_q \bar{\boldsymbol{\Lambda}}_q^\dagger \mathbf{M}_q \bar{\boldsymbol{\Lambda}}_q$, where $\bar{\boldsymbol{\Lambda}}_q^\dagger = (\Lambda_q^* \Lambda_{-q})$ and $\mathbf{M}_q$ is the inverse fluctuation propagator [22–27]. Simplifying the notation by denoting $\xi_{s,\mathbf{k}+\mathbf{q}/2}$ by ξ; $\xi_{s',-\mathbf{k}+\mathbf{q}/2}$ by ξ'; $E_{s,\mathbf{k}+\mathbf{q}/2}$ by E; $E_{s',-\mathbf{k}+\mathbf{q}/2}$ by E'; and $\hat{\mathbf{d}}_{\pm\mathbf{k}+\mathbf{q}/2}$ by $\hat{\mathbf{d}}_\pm$, and defining the functions $u^2 = (1+\xi/E)/2$; $u'^2 = (1+\xi'/E')/2$; $v^2 = (1-\xi/E)/2$; $v'^2 = (1-\xi'/E')/2$; $f = 1/(e^{E/T}+1)$; and $f' = 1/(e^{E'/T}+1)$, a compact way to write the matrix elements of $\mathbf{M}_q$ is [22,23]

$$M_q^{11} = \frac{1}{U} + \frac{1}{4}\sum_{ss'\mathbf{k}}\left(1 - ss'\hat{\mathbf{d}}_+\cdot\hat{\mathbf{d}}_-\right) \times \left[(1-f-f')\left(\frac{u^2u'^2}{i\nu_n - E - E'} - \frac{v^2v'^2}{i\nu_n + E + E'}\right) + (f-f')\left(\frac{v^2u'^2}{i\nu_n + E - E'} - \frac{u^2v'^2}{i\nu_n - E + E'}\right)\right], \tag{A.5}$$

$$M_q^{12} = \frac{1}{4}\sum_{ss'\mathbf{k}}\left(1 - ss'\hat{\mathbf{d}}_+\cdot\hat{\mathbf{d}}_-\right) \times \left[(1-f-f')\left(\frac{uvu'v'}{i\nu_n + E + E'} - \frac{uvu'v'}{i\nu_n - E - E'}\right) + (f-f')\left(\frac{uvu'v'}{i\nu_n + E - E'} - \frac{uvu'v'}{i\nu_n - E + E'}\right)\right]. \tag{A.6}$$

The remaining elements are related via $M_q^{22} = M_{-q}^{11}$ and $M_q^{21} = M_q^{12}$. We note that while M_q^{12} is even both under $\mathbf{q} \to -\mathbf{q}$ and $i\nu_n \to -i\nu_n$, M_q^{11} is even only under $\mathbf{q} \to -\mathbf{q}$.

While calculating the collective excitations, it is useful to represent $\Lambda_q = \alpha_q e^{i\gamma_q}$ in terms of real functions α_q and γ_q, and associate $\lambda_q = \sqrt{2}\alpha_q\cos(\gamma_q)$ with the amplitude degrees of freedom and $\theta_q = \sqrt{2}\alpha_q\sin(\gamma_q)$ with the phase ones in the small γ_q limit. This procedure corresponds to a unitary transformation $\Lambda_q = (\lambda_q + i\theta_q)/\sqrt{2}$, where λ_q and θ_q are real functions. Furthermore, assuming $\lambda_{-q} = \lambda_q^*$ and $\theta_{-q} = \theta_q^*$, we find

$$S_2 = \frac{1}{2T}\sum_q \Theta_q^\dagger \begin{pmatrix} M_{q,E}^{11} + M_q^{12} & iM_{q,O}^{11} \\ -iM_{q,O}^{11} & M_{q,E}^{11} - M_q^{12} \end{pmatrix}\Theta_q, \tag{A.7}$$

where we denote $\Theta_q^\dagger = (\lambda_q^* \theta_q^*)$, and separate $M_q^{11} = M_{q,E}^{11} + M_{q,O}^{11}$ in terms of an even function $M_{q,E}^{11} = (M_q^{11} + M_q^{22})/2$ in $i\nu_n$ and an odd one $M_{q,O}^{11} = (M_q^{11} - M_q^{22})/2$, and use $M_q^{12} = M_q^{21}$ [22–27]. The phase-only action given in Eq. (5) is derived by integrating out the amplitude fields, and vice versa for the Eq. (6). We note that since the quasiparticle–quasihole terms with the prefactor $(f - f')$ have the usual Landau singularity for $q \to (\mathbf{0}, 0)$ causing the collective modes to decay into the two-quasiparticle continuum, a small q expansion is possible only in two cases: (i) just below the critical SF transition temperature provided $\Delta_0 \to 0 \ll i\nu_n \to \omega$ [7], and (ii) at $T = 0$. In this work, we are interested in the latter case [21].

References

[1] J.P. Provost, G. Vallee, Riemannian structure on manifolds of quantum states, Commun. Math. Phys. 76 (1980) 289.
[2] M.V. Berry, The Quantum Phase, Five Years After in Geometric Phases in Physics, World Scientific, Singapore, 1989,
[3] D.J. Thouless, Topological Quantum Numbers in Nonrelativistic Physics, World Scientific, Singapore, 1998.
[4] D. Xiao, M.C. Chang, Q. Niu, Berry phase effects on electronic properties, Rev. Modern Phys. 82 (2010) 1959.
[5] X.L. Qi, S.C. Zhang, Topological insulators and superconductors, Rev. Modern Phys. 83 (2011) 1057.
[6] M. Iskin, Exposing the quantum geometry of spin–orbit coupled Fermi superfluids, Phys. Rev. A 97 (2018) 063625.
[7] M. Iskin, Quantum metric contribution to the pair mass in spin–orbit coupled Fermi superfluids, Phys. Rev. A 97 (2018) 033625.
[8] R. Resta, The insulating state of matter: A geometrical theory, Eur. Phys. J. B 79 (2011) 121.
[9] X. Tan, D.W. Zhang, Z. Yang, J. Chu, Y.Q. Zhu, D. Li, X. Yang, S. Song, Z. Han, Z. Li, Y. Dong, H.F. Yu, H. Yan, S.L. Zhu, Y. Yu, Experimental measurement of the quantum metric tensor and related topological phase transition with a superconducting qubit, Phys. Rev. Lett. 122 (2019) 210401.
[10] M. Yu, P. Yang, M. Gong, Q. Cao, Q. Lu, H. Liu, M.B. Plenio, F. Jelezko, T. Ozawa, N. Goldman, S. Zhang, J. Cai, Experimental measurement of the complete quantum geometry of a solid-state spin system, Natl. Sci. Rev. (2019) http://dx.doi.org/10.1093/nsr/nwz193, nwz193.
[11] S. Peotta, Törmä, Superfluidity in topologically nontrivial flat bands, Nature Commun. 6 (2015) 8944.
[12] L. Liang, T.I. Vanhala, S. Peotta, A. Siro, Törmän, Band geometry, Berry curvature, and superfluid weight, Phys. Rev. B 95 (2017) 024515.
[13] X. Hu, T. Hyart, D.I. Pikulin, E. Rossi, Geometric and conventional contribution to superfluid weight in twisted bilayer graphene, Phys. Rev. Lett. 123 (2019) 237002.
[14] A. Julku, T.J. Peltonen, L. Liang, T.T. Heikkilä, Törmä, Superfluid weight and Berezinskii-Kosterlitz–Thouless transition temperature of twisted bilayer graphene, Phys. Rev. B 101 (2020) 060505.
[15] F. Xie, Z. Song, B. Lian, B.A. Bernevig, Topology-bounded superfluid weight in twisted bilayer graphene, Phys. Rev. Lett. 123 (2020) 237002.

[16] P. Wang, Z. Yu, Z. Fu, J. Miao, L. Huang, S. Chai, H. Zhai, J. Zhang, Spin–orbit coupled degenerate Fermi gases, Phys. Rev. Lett. 109 (2012) 095301.
[17] L.W. Cheuk, A.T. Sommer, Z. Hadzibabic, T. Yefsah, W.S. Bakr, M.W. Zwierlein, Spin-injection spectroscopy of a spin-orbit coupled Fermi gas, Phys. Rev. Lett. 109 (2012) 095302.
[18] R.A. Williams, M.C. Beeler, L.J. LeBlanc, K. Jiménez-García, I.B. Spielman, Raman-induced interactions in a single-component Fermi gas near an s-wave feshbach resonance, Phys. Rev. Lett. 111 (2013) 095301.
[19] L. Huang, Z. Meng, P. Wang, P. Peng, S.L. Zhang, L. Chen, D. Li, Q. Zhou, J Zhang, Experimental realization of a two-dimensional synthetic spin–orbit coupling in ultracold Fermi gases, Nature Phys. 12 (2016) 540.
[20] Z. Meng, L. Huang, P. Peng, D. Li, L. Chen, Y. Xu, C. Zhang, P. Wang, J. Zhang, Experimental observation of a topological band gap opening in ultracold Fermi gases with two-dimensional spin-orbit coupling, Phys. Rev. Lett. 117 (2016) 235304.
[21] This work is complementary to our recent works. In [6], we used a linear response theory and identified the SF-density tensor from the response of the thermodynamic potential to an infinitesimal superfluid flow. In [7], we derived the time-dependent Ginzburg-Landau theory near the critical temperatures, and identified the effective-mass tensor of the Cooper pairs by making an analogy with the Gross–Pitaevskii theory of the corresponding molecular Bose gas.
[22] J.R. Engelbrecht, M. Randeria, C.A.R. Sá de Melo, BCS to Bose crossover: Broken-symmetry state, Phys. Rev. B 55 (1997) 15153.
[23] C.A.R. Iskin, BCS-BEC crossover of collective excitations in two-band superfluids, Phys. Rev. B 72 (2005) 024512.
[24] L. He, X.G. Huang, BCS-BEC crossover in three-dimensional Fermi gases with spherical spin–orbit coupling, Phys. Rev. B 86 (2012) 014511.
[25] J.P. Vyasanakere, V.B. Shenoy, Collective excitations, emergent galilean invariance, and boson-boson interactions across the BCS-BEC crossover induced by a synthetic Rashba spin-orbit coupling, Phys. Rev. A 86 (2012) 053617.
[26] L. He, X.G. Huang, Unusual zeeman-field effects in two-dimensional spin–orbit-coupled Fermi superfluids, Phys. Rev. A 86 (2012) 043618.
[27] L. He, X.G. Huang, Superfluidity and collective modes in Rashba spin-orbit coupled Fermi gases, Ann. Physics 337 (2013) 163.
[28] To be more precise, one needs to derive the characteristic equation up to fourth order in the expansion, e.g. $\beta_5\omega^4 + \sum_{ijkl}\beta_4^{ijkl}q_iq_jq_kq_l + \sum_{ij}\beta_3^{ij}\omega^2q_iq_j + \beta_2\omega^2 + \sum_{ij}\beta_1^{ij}q_iq_j = 0$, such that $x_{ij} = -\beta_1^{ij}/\beta_2, \omega_0^2 = -\beta_2/\beta_5$ and $y_{ij} = -\beta_3^{ij}/\beta_5 + \beta_1^{ij}/\beta_2$. While our quadratic expansion fully determines x_{ij}, we neglect the additional corrections to ω_0^2 and y_{ij} coming from the higher order terms.
[29] In contrast to the dispersion of the Goldstone mode that we calculate in this paper, the correct dispersion of the Higgs mode requires a more special treatment as recently discussed in H. Kurkjian, S.N. Klimin, J. Tempere, Y. Castin, Pair-Breaking Collective Branch in BCS Superconductors and Superfluid Fermi Gases, Phys. Rev. Lett. 122 (2019) 093403.
[30] The familiar expressions for the one-band coefficients can be written as [22] $Q_{ij} = Q_{ij}^{\rm intra} = \sum_{\mathbf{k}}[\xi_{\mathbf{k}}\partial^2\xi_{\mathbf{k}}/(\partial k_i\partial k_j) - (\partial\xi_{\mathbf{k}}/\partial k_i)(\partial\xi_{\mathbf{k}}/\partial k_j)(1-3\Delta_0^2/E_{\mathbf{k}}^2)]/(8E_{\mathbf{k}}^3)$ and $C_{ij} = C_{ij}^{\rm intra} = \sum_{\mathbf{k}}[\xi_{\mathbf{k}}(1-3\Delta_0^2/E_{\mathbf{k}}^2)\partial^2\xi_{\mathbf{k}}/(\partial k_i\partial k_j) - (\partial\xi_{\mathbf{k}}/\partial k_i)(\partial\xi_{\mathbf{k}}/\partial k_j)(1-10\Delta_0^2\xi_{\mathbf{k}}^2/E_{\mathbf{k}}^4)]/(8E_{\mathbf{k}}^3)$, and our intraband coefficients recover them in the absence of a SOC when $d_{\mathbf{k}} \to 0$.
[31] M. Iskin, Superfluid stiffness for the attractive hubbard model on a honeycomb optical lattice, Phys. Rev. A 99 (2019) 023608.
[32] Iskin, Origin of flat-band superfluidity on the mielke checkerboard lattice, Phys. Rev. A 99 (2019) 053608.
[33] V.M. Edelstein, Magnetoelectric effect in polar superconductors, Phys. Rev. Lett. 75 (1995) 2004.
[34] L.P. Gorkov, E.I. Rashba, Superconducting 2D system with lifted spin degeneracy: Mixed singlet-triplet state, Phys. Rev. Lett. 87 (2001) 037004.